Universal transport properties of open microwave cavities with and without time-reversal symmetry

H. Schanze and H.-J. Stöckmann
Fachbereich Physik der Philipps-Universität Marburg, D-35032 Marburg, Germany

M. Martínez-Mares
Departamento de Física, UAM-Iztapalapa, Avenida San Rafael Atlixco 186, Col. Vicentina, 09340 México, Distrito Federal, Mexico and Instituto de Física, Universidade do Estado do Rio de Janeiro, Rua São Francisco Xavier 524, 20550-900 Rio de Janeiro, Brazil

C. H. Lewenkopf
Instituto de Física, Universidade do Estado do Rio de Janeiro, R. São Francisco Xavier 524, 20550-900 Rio de Janeiro, Brazil
(Received 26 July 2004; published 28 January 2005)

We measure the transmission through asymmetric and reflection-symmetric chaotic microwave cavities in dependence on the number of attached waveguides. Ferrite cylinders are placed inside the cavities to break time-reversal symmetry. The phase-breaking properties of the ferrite and its range of applicability are discussed in detail. We use the random matrix theory accounting for absorption effects to calculate the universal distribution of transmission coefficients T and their energy derivatives $dT/d\varepsilon$. Using the absorption strength as a fitting parameter, we find good agreement between universal transmission fluctuations predicted by the theory and the experimental data.

DOI: 10.1103/PhysRevE.71.016223 PACS number(s): 05.45.Mt, 03.65.Nk, 73.23.−b

I. INTRODUCTION

There has been much theoretical interest in the universal transmission fluctuations through ballistic chaotic systems over recent years [1,2]. This activity is partially driven by recent experiments on electronic conductance in open quantum dots at very low temperatures. In the absence of inelastic scattering, according to the Landauer formula, the conductance is proportional to the total transmission. Assuming that the statistical transmission properties of chaotic scattering systems are well described by the random-matrix theory [3–5], analytical results on the distribution of transmission and reflection coefficients, as well as on other related quantities, are readily obtained [1].

Remarkably, there are very few ballistic experimental systems that clearly show the universal transmission (or conductance) fluctuations predicted by random-matrix theory. Universal conductance fluctuations in quantum dots [6] are already weak at temperatures of the order of the mean level (resonance) spacing. (In practice, for a typical semiconductor quantum dots of submicrometer size, the temperature should be smaller than 100 mK.) This is mainly due to the thermal smearing [7], but dephasing also plays a significant role [8]. The latter can be incorporated into the random-matrix modeling by introducing additional phase-randomizing channels [9]. Hence, theoretical clear-cut predictions of the transmission fluctuation dependence on the number of incoming and outgoing channels [10,11] are hardly observed. Despite these difficulties, quantum dots provided the first clear fingerprint of time-reversal symmetry breaking in the transmission distributions [12]. Theory and experiment showed an excellent agreement once the dephasing time was accounted for as a free parameter.

An alternative way to study universal transmission fluctuations is provided by microwave techniques. Transmission is directly measured in microwave experiments, and it is easy to fabricate cavities of any shape. Hence, this approach is ideally suited to verify theoretical predictions on transmission distributions. The first experiment of this type was performed by Doron *et al.* [13]. This may be considered as an experimental equivalent of the work by Jalabert *et al.* [14] on conductance fluctuations in essentially the same system. A study aiming at the channel number dependence and the influence of time-reversal symmetry breaking is our own work [15]. For the sake of completeness we would like to mention that there are two further microwave experiments concentrating on nonuniversal aspects of transmission [16].

Another quantity we shall examine in detail is the energy derivative of the transmission, $dT/d\varepsilon$. The motivation stems from the study of the thermopower in electronic systems which was shown to be proportional to the derivative of the conductance (or transmission) with respect to the Fermi energy (see, e.g., Ref. [17] for details and further references). The theory predicts a qualitative difference between diffusive and ballistic systems. Whereas for a disordered wire the distribution of $dT/d\varepsilon$ is predicted to be Lorentzian, for a chaotic quantum dot one expects a distribution with a cusp at $\varepsilon=0$ [17,18].

The study of universal transmission fluctuations using microwave experiments has its own characteristic limitations. It is not trivial to break time-reversal symmetry in microwave systems. In contrast, theoretical results are usually available for systems with broken time-reversal symmetry only, since for systems with time-reversal symmetry analytical progress faces formidable technical problems. One way to break time-reversal symmetry in microwave systems is to introduce fer-

rites into the resonator [19,20]. By applying an external magnetic field the electrons in the material perform a Larmor precession, thus introducing a chirality into the system, the precondition for breaking time-reversal symmetry. It will become clear in what follows that this effect is unavoidably accompanied by strong absorption.

Thus, in microwave experiments there is either no time-reversal symmetry breaking, or strong absorption, or both. Although, meanwhile, there are a number of theoretical works that address absorption effects in microwave cavities [21–24], we will show that such analysis is not yet complete.

Last, but not least, the coupling between the cavity and the waveguides is usually not perfect (or ideal) in the experiments. Nonideal contacts mean that part of the incoming flux is promptly reflected at the entrance of the cavity and, hence, it is not resonant. (The same holds for quantum dots and leads.) For the sake of simplicity most of the theoretical studies assume perfect coupling. Accounting for nonideal coupling is not difficult [1,25,26]. The problem, however, is that the quality of the contacts depend formally on the average S matrix. In other words, the phases of the S matrix are needed to quantitatively determine the coupling strength. This information, in general, is not available [27]. We discuss this issue in our analysis.

This paper is organized as follows. In Sec. II we describe the experimental setup and discuss how the addition of ferrite cylinders to the microwave cavities breaks time-reversal symmetry. The phase-breaking features of the ferrite and its absorption characteristics are discussed in the Appendix. In Sec. III we present the key elements of the statistical theory for transmission fluctuations in ballistic chaotic systems. Section IV is devoted to the statistical analysis of our experimental data. We vastly expand a previously presented analysis of transmission fluctuations through asymmetric cavities [15]. Here we analyze additional data on systems with reflection symmetry, expected to show different universal transmission fluctuations from those without reflection symmetry [28,29]. We also discuss the distribution of the derivative of the transmission with respect to energy, $dT/d\varepsilon$. Our conclusions and an outlook on the open problems are presented in Sec. V.

II. THE EXPERIMENT

Two different cavities were used in the experiment: an asymmetric and a symmetric one [30]. Their shapes, shown in Fig. 1, are inspired by the Sinai billiard, a paradigm of classical chaotic motion. Wedgelike boundaries are used to eliminate the bouncing ball modes in the cavity, but do not prevent their presence in the cavity "arms." Bouncing ball modes are in correspondence with marginally stable classical motion. They are known to cause nonuniversal spectral correlations observed at large energy (or frequency), unlikely to be relevant for our study.

The height of the cavities is $h=7.8$ mm, i.e., both are quasi-two-dimensional for frequencies ν below $\nu_{\max}=c/2h=19.2$ GHz. Two commercially available waveguides were attached on both the entrance and the exit side. The cutoff frequency for the first mode is at $\nu_1=c/2w=9.5$ GHz where

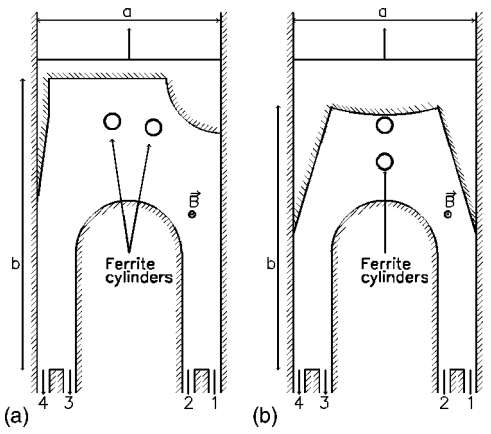

FIG. 1. Sketch of the microwave cavities used in the experiments. (a) The asymmetric cavity has $a=237$ mm and b can vary from 375 to 425 mm. (b) The symmetric one has the same a, while b ranges from 340 to 390 mm. The arrows indicate where the ferrite cylinders are placed. The entrance and exit waveguides are denoted by (1,2) and (3,4), respectively.

$w=15.8$ mm is the width of the waveguides. Above $\nu_2=18.9$ GHz a second mode becomes propagating. All measurements have been performed in the frequency regime where there is just a single propagating mode. The transmission coefficients were measured for all combinations of entrance and exit waveguides. Figure 2 shows a typical transmission spectrum. By varying the length b of the resonator 100 different spectra were taken, which were superimposed to improve statistics and to eliminate possible nongeneric structures. A similar procedure has already been used in quantum dot experiments [8,12].

To break time-reversal symmetry we make use of the peculiar ferrite reflection properties. We place two hollow ferrite cylinders with radius $r=10$ mm and thickness $d=1$ mm inside the cavities. We decided to use two such cylinders to make sure that all microwaves transmitted by the cavity are also scattered by the ferrite. This choice was very successful, as will become evident from the results. Therefore we did not vary systematically the number of ferrite inserts, which would require a very large additional effort. The cylinder magnetization is varied by applying an external magnetic field. At an induction of $B=0.475$ T the ferromagnetic reso-

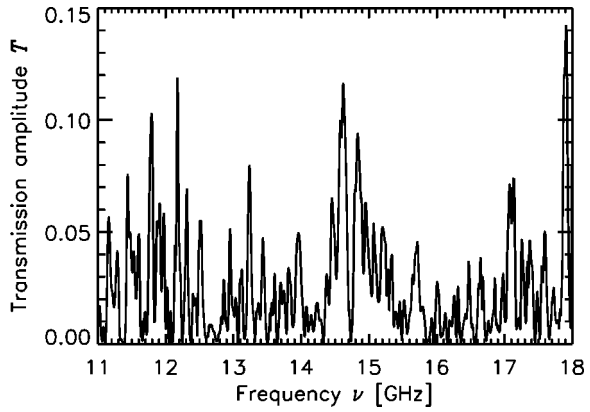

FIG. 2. Typical transmission spectrum (asymmetric cavity).

nance is centered at about 15.5 GHz. The electrons in the ferrite perform a Larmor precession about the axis of the magnetic field. At the Larmor frequency the ferromagnetic resonance is excited giving rise to a strong microwave absorption. This is, of coarse, unwanted. Moving to frequencies located at the tails of the ferromagnetic resonance, the microwaves are partially reflected and acquire a phase shift depending on the sign of the propagation. The ferrite cylinder has thus a similar effect on the photons as an Aharonov-Bohm flux line in a corresponding electron system. This correspondence has already been explored to study persistent currents using a microwave analog [31].

This method to break time-reversal symmetry has an obvious and unavoidable limitation: We have to move away from the ferromagnetic resonance frequency to avoid strong absorption, but we also have to stay close enough to observe a significant phase-breaking effect. In the present experiment, the optimal frequencies occur on a quite narrow interval between 13.5 and 14.0 GHz, but still the typical linewidths are about half an order of magnitude larger than in the absence of the ferrite inserts. The Appendix gives a quantitative description of the phase-breaking mechanism due to the ferrite cylinders. Specific properties of the employed ferrite, which are useful for the understanding of the experimental data, are also discussed.

III. STATISTICAL THEORY

There are two standard statistical theories that describe universal transmission fluctuations of ballistic systems. One is the *S*-matrix information-theoretical theory [32], tailormade to calculate transmission distributions. The other method, where the statistical *S* matrix is obtained by modeling the scattering region by a stochastic Hamiltonian [2], is suited to the computation of energy and parametric transmission correlation functions. Both approaches were proven to be strictly equivalent in certain limits [4]. Complementing this result, there is numerical evidence supporting that the equivalence is general [7]. Here we use both methods: Our analytical results (mainly for variances) are obtained from the information-theoretical approach, whereas the numerical simulations (for the full distributions) are based on the stochastic Hamiltonian one.

We model the transmission flux deficit due to absorption by a set of N_ϕ nontransmitting channels coupled to the cavity. We consider N_1 and N_2 propagating modes at the entrance and the exit waveguides, respectively. The resulting scattering process is described by the block structured *S* matrix

$$S = \begin{pmatrix} S_{11} & S_{12} & S_{1\phi} \\ S_{21} & S_{22} & S_{2\phi} \\ S_{\phi 1} & S_{\phi 2} & S_{\phi\phi} \end{pmatrix} \equiv \begin{pmatrix} & \widetilde{S} & S_{1\phi} \\ & & S_{2\phi} \\ S_{\phi 1} & S_{\phi 2} & S_{\phi\phi} \end{pmatrix}. \qquad (1)$$

Here the set of indices $\{1\},\{2\}$ label the N_1, N_2 propagating modes at the waveguides, while the set $\{\phi\}$ labels the N_ϕ absorption channels. Transmission and reflection measurements, necessarily taken at the waveguides, access directly only the $\widetilde{S}$-matrix elements.

Of particular experimental interest is the total transmission coefficient, namely,

$$T = \sum_{\substack{a\in 2 \\ b\in 1}} T_{ab} \quad \text{with} \quad T_{ab} \equiv |\widetilde{S}_{ab}|^2. \qquad (2)$$

The absorption at each N_ϕ channel can be quantified [33] by $\Gamma_\phi = 1 - |\langle S_{\phi\phi}\rangle|^2$, where $\langle\cdots\rangle$ indicates an ensemble average (described below). A given ϕ channel is weakly coupled (or provides little absorption) if $\Gamma_\phi \ll 1$, whereas if $\Gamma_\phi = 1$ the cavity is perfectly coupled to the channel ϕ and the corresponding absorption is maximal. We take the limits $N_\phi \gg 1$ (many possible absorption channels) and $\Gamma_\phi \ll 1$, while keeping $N_\phi \Gamma_\phi = \Gamma$ constant. In this way we mimic the absorption processes occurring over the entire cavity surface, expressing their strength by a single parameter Γ [33]. This modeling, used in the numerical simulations described below, is equivalent to adding an imaginary part to the energy in the *S* matrix [34], a standard way to account for a finite *Q* value [13].

We obtain the distributions $P_\beta(T)$ by numerical simulation. To that end, we employ the Hamiltonian approach to the statistical *S* matrix, namely,

$$S(\varepsilon) = \mathbb{1} - 2\pi i W^\dagger (\varepsilon - H + i\pi W W^\dagger)^{-1} W, \qquad (3)$$

where *H* is the matrix of dimension $M \times M$ that describes the resonant states. *H* is taken as a member of the Gaussian orthogonal (unitary) ensemble for the (broken) time-reversal symmetric case. The matrix *W* of dimension $M \times (N_1 + N_2 + N_\phi)$ contains the channel-resonance coupling matrix elements and ε is the energy. This *S*-matrix parametrization is entirely equivalent to the *K*-matrix formulation recently used by Kogan and collaborators [21]. Since the *H* matrix is statistically invariant under orthogonal ($\beta = 1$) or unitary ($\beta = 2$) transformations, the statistical properties of *S* depend only on the mean resonance spacing Δ, determined by *H*, and the traces of $W^\dagger W$. Maximizing the average transmission, or assuming perfect coupling, is equivalent to setting $\mathrm{tr}(W^\dagger W) = \Delta/\sqrt{\pi}$ [35]. The Hamiltonian approach can be used, in principle, to study any number *N* of open channels. We find it convenient to express our results in terms of $E = \varepsilon/\Delta$, i.e., all energies *E* are given in units of the mean resonance spacing Δ. Later the experimental data will be scaled likewise. The Δ in the experiments has been estimated from the Weyl formula for closed resonators, including the surface term.

Some words about our model are in order. One can describe the transmission in terms of trajectories scattered by the cavity in a semiclassical picture. In this scenario, the time-reversal symmetry is broken as the actions of the trajectories acquire a sufficiently large additional time-reversal symmetry (TRS) breaking contribution due to the ferrite cylinders. For full TRS breaking, the phase shifts (changes in action, measured in units of $\hbar$) should be distributed between 0 and 2π. For that matter it is not important whether this is achieved continuously, as for an electron in a magnetic field, or discontinuously, as in our case. Actually, our theoretical modeling uses a different, but equivalent, picture. It assumes a Hamiltonian with broken TRS. The magnitude of the TRS breaking matrix elements depends on the resonance "wave

function" amplitudes inside the ferrite, where a local time-reversal symmetry breaking potential acts. Wave functions corresponding to distinct states of a chaotic system are uncorrelated, providing a heuristic justification for the model. Similar arguments apply to the absorption that occurs at the walls of the resonator. Our model assumes that the different absorption processes can, in principle, be labeled in terms of its asymptotic radiation properties, defining the absorption channels. Although of little use for a detailed microscopic calculation, this description in terms of effective channels in Hilbert space is very practical for our statistical analysis.

The numerical simulations are straightforward. For every realization of H we invert the propagator and compute $S(E)$ for energy values close to the center of the band, $E=0$, where the level density is approximately constant. The dimension of H is fixed as $M=100$ to 200, depending on the number of channels N. The choice of M represents the compromise between having a wide energy window for the statistics (large M) and fast computation (small M). For each value of Γ we obtain very good statistics with 10^4-10^5 realizations.

The full distribution of the transmission energy derivatives, $\widetilde{P}_\beta(dT/dE)$, is obtained by numerical simulations. This is a simple extension of the numerical procedure described above. We compute dS/dE directly from

$$\frac{dS}{dE} = 2\pi i W^\dagger (E - H + i\pi W W^\dagger)^{-2} W, \tag{4}$$

at the same time as $S(E)$ is calculated.

We also analyze the fluctuations of the transmission coefficient energy derivative dT/dE. We use the information-theoretical approach to analytically compute moments of dT/dE. For that purpose we express dS/dE in terms of the S matrix itself and a symmetrized form of the Wigner-Smith time-delay matrix Q_E [36], namely,

$$\frac{dS}{dE} = \frac{i}{\hbar} S^{1/2} Q_E S^{1/2}. \tag{5}$$

Thanks to the well known statistical properties of Q_E matrices, the computation of $\langle (dT_{ab}/dE)^2 \rangle$ is possible [37]. We note that Eq. (5) is strictly valid only when all channels are ideally coupled to the scatterer. That is, $\Gamma_c = 1$ where c can be either a waveguide or an absorbing channel. Hence, $\Gamma = N_\phi \Gamma_\phi$ is an integer number.

Note that the only parameters of the statistical theory are the local mean resonance spacing Δ, the number of channels N, and the absorption parameter Γ. In what follows we analyze the cases of asymmetric and symmetric cavities.

Asymmetric cavities

The presented formalism is readily suited for asymmetric chaotic cavities, since to this point only stochasticity and orthogonal (time-reversal) or unitary (broken time-reversal) symmetry are assumed. Additional symmetries require special S-matrix parametrizations.

Figure 3 shows $P(T)$ for the $N=1$ and 2 cases for various values of the absorption Γ. One can nicely observe how the distributions for zero absorption [10] evolve to an exponential ($N=1$) or a convolution of exponentials ($N=2$) as the absorption strength Γ increases. For $N=1$ our simulations are in excellent agreement (within the statistical error and almost indistinguishable in the scale of the graph) with the analytical expression obtained in Refs. [15,34]. The comparison between our simulations and the analytical distributions for the case $N=2$ without absorption is also excellent. This consistency test makes us confident in the numerical procedure.

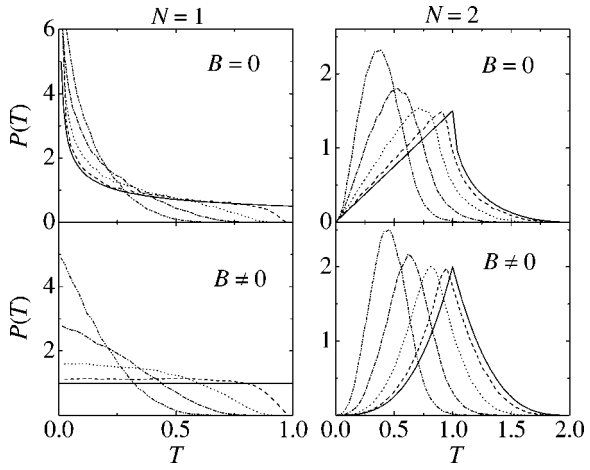

FIG. 3. Transmission distribution $P(T)$ for asymmetric chaotic cavities with $N=1$ and 2 open channels, both cases with ($B=0$) and without ($B\neq 0$) time-reversal symmetry. We consider different absorption parameters Γ: 0 (solid), 0.25 (dashed), 1 (dotted), 2.5 (dash-dotted), and 5 (dash-dot-dotted).

For strong absorption $\Gamma \gg 1$, we find strong numerical evidence that the distribution of individual channel-channel transmission energy derivatives, dT_{ab}/dE, is exponential, namely,

$$\widetilde{P}_\beta(dT_{ab}/dE) = \frac{\lambda_\beta}{2} \exp\left(-\lambda_\beta \left| \frac{dT_{ab}}{dE} \right| \right), \tag{6}$$

where λ_β depends on Γ, but not the channel indices a and b. Furthermore, in this regime we find that the dT_{ab}/dE for different pairs of channels are uncorrelated [37]. We conclude that either this distribution is insensitive to dynamical channel-channel correlations, or such correlations are insignificant in our billiards. Figure 4 presents results for typical experimental values. For independent dT_{ab}/dE, the distribution of dT/dE for $N=2$ is easily obtained from Eq. (6) and reads

$$\widetilde{P}_\beta(dT/dE) = \frac{\lambda_\beta}{96} \exp\left(-\lambda_\beta \left| \frac{dT}{dE} \right| \right) \times \left(\lambda_\beta^3 \left| \frac{dT}{dE} \right|^3 + 6\lambda_\beta^2 \left| \frac{dT}{dE} \right|^2 + 15\lambda_\beta \left| \frac{dT}{dE} \right| + 15 \right). \tag{7}$$

It remains to relate λ_β to Γ. This is done by computing $\langle (dT_{ab}/dE)^2 \rangle$. The latter can be analytically calculated using the energy derivative of the S matrix, Eq. (5), and reads [37]

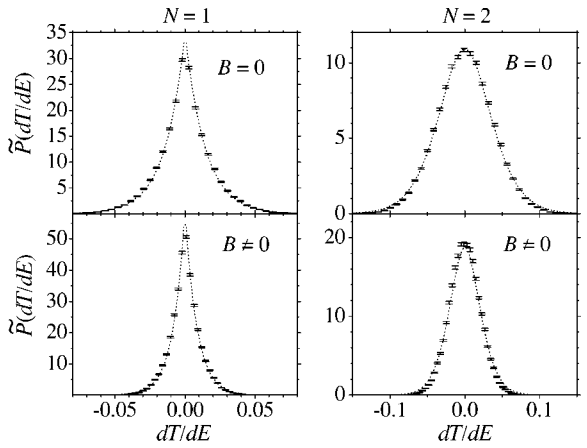

FIG. 4. Distributions of dT/dE for asymmetric cavities. Here and in all subsequent figures the energy is expressed in units of the mean level spacing Δ, namely, $E=\varepsilon/\Delta$. For $N=1$ the distributions agree with Eq. (6) (dotted line), while for $N=2$ they follow Eq. (7) (dotted line).

$$\left\langle \left(\frac{dT_{ab}}{dE} \right)^2 \right\rangle = \frac{8\pi^2}{\alpha^2(\alpha+1)^2} \frac{\alpha^2+\alpha-2+4(2-\beta)}{\alpha^2+\alpha-2-4(2-\beta)}, \qquad (8)$$

where $\alpha=N_1+N_2+\Gamma$. Recalling that $\langle (dT_{ab}/dE)^2 \rangle = 2/\lambda_\beta^2$ we find λ_β as a function of Γ. As pointed out below Eq. (5), the above formula is valid only for integer values of Γ. Throughout this study we interpolate our formulas for the variances of dT/dE for noninteger values of Γ.

In Fig. 4 we compare the approximation $\widetilde{P}_\beta(dT/dE)$, where λ_β is calculated as described above, with a direct numerical simulation. The agreement is rather good.

Symmetric cavities

The influence of absorption on the transmission fluctuations is even more pronounced in billiards with reflection symmetry. In the absence of absorption the transmission distributions for reflection-symmetric cavities were already analytically computed. The most salient features are the following. When time-reversal symmetry is preserved, the theory predicts that the transmission distribution $P(T)$ for reflection-symmetric cavities remains invariant when T is substituted by $1-T$ [38]. On the other hand, for broken time-reversal symmetry, $P(T)$ coincides with the one for the *asymmetric* case, but with T replaced by $1-T$ [29].

To account for the reflection symmetry, it is sufficient to consider the S matrix with the block structure [38]

$$S = \begin{bmatrix} \frac{1}{2}(S_1+S_2) & \frac{1}{2}(S_1-S_2) \\ \frac{1}{2}(S_1-S_2) & \frac{1}{2}(S_1+S_2) \end{bmatrix}, \qquad (9)$$

where S_1 and S_2 are unitary (and symmetric for $\beta=1$) $N_T/2 \times N_T/2$ matrices with $N_T=2N+N_\phi$. Both S_1 and S_2 have the structure given by Eq. (1).

The transmission coefficient now reads

$$T = \frac{1}{4} \sum_{a,b=1}^{N} |[S_1]_{ab} - [S_2]_{ab}|^2 \equiv \sum_{a,b=1}^{N} \sigma_{ab}. \qquad (10)$$

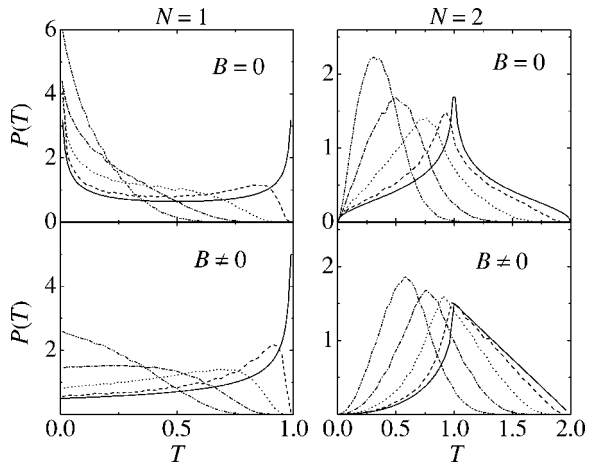

FIG. 5. Symmetric cavity transmission distributions $P(T)$ for the one- and two-channel cases. For $B=0$ we consider $\Gamma=0$, 0.5, 2, 2.5, and 10, corresponding to the solid, dashed, dotted, dash-dotted, and dash-dot-dotted lines, respectively. For the case of broken time-reversal symmetry, $B\neq 0$, the same symbols refer to $\Gamma=0$, 0.25, 1, 2.5, and 5.

We numerically generate $P_\beta(T)$ and $\widetilde{P}_\beta(dT/dE)$ using the Hamiltonian approach to the S matrix, Eqs. (3) and (5). Now two statistically independent matrices S_1 and S_2 are required. Here we chose the dimension of H to be $M=50$. For each value of Γ we ran 10^5 realizations. We checked the quality of our simulations with the analytical results avaliable for $\Gamma=0$ and verified an excellent agreement within the statistical error.

Figure 5 contrasts $P_\beta(T)$ obtained analytically for zero absorption [29] with our numerical simulations for different values of Γ. Our analysis is restricted to $N=1$ and 2, as before. We observe that with increasing Γ the fingerprints of the reflection symmetry fade away, and the distributions become quite similar to those of asymmetric cavities.

As in the asymmetric case, for the strong absorption regime, $\Gamma \gg 1$, our numerical simulations strongly suggest that the distribution of the energy derivative of individual channel-channel transmission coefficients $\widetilde{P}_\beta(dT_{ab}/dE)$ is exponential. However, in distinction from the asymmetric case, here the exponential law depends on the channels: The reflection symmetry (see Fig. 1) makes the channels (1,4) and (2,3) indistinguishable. Accordingly, we find that the "diagonal" coefficients T_{14} and T_{23}, denoted by σ_{ab}^{d}, and the "off-diagonal" ones T_{24} and T_{13}, denoted by σ_{ab}^{o} have different variance. The second moment of the diagonal $d\sigma_{ab}^{\mathrm{d}}/dE$ is [37]

$$\left\langle \left(\frac{d\sigma_{ab}^{\mathrm{d}}}{dE} \right)^2 \right\rangle = \frac{4\pi^2}{(\alpha'-2)\alpha'^2(\alpha'+1)^2} \left[\frac{\alpha'(\alpha'-1)(7\beta-6)}{\alpha'+3} + \frac{(\alpha'^2+\alpha'+2)(2-\beta)}{\alpha'+1} \right] \qquad (11)$$

whereas the off diagonal is

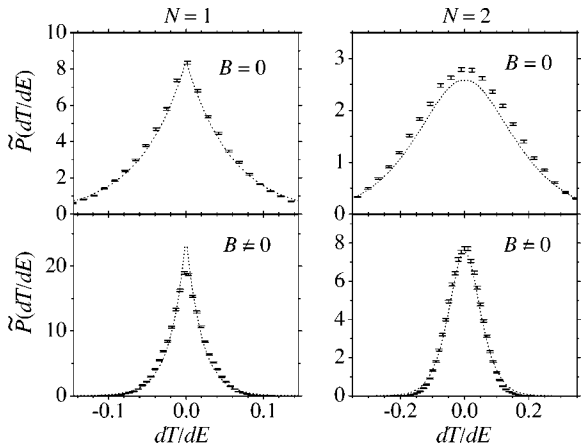

FIG. 6. Transmission energy derivative distributions for the symmetric chaotic cavities. The points represent the results of the simulations for $\Gamma=18$ (22) for $B=0$ ($B\neq 0$) for $N=1$; $\Gamma=14$ (18) for $B=0$ ($B\neq 0$) for $N=2$. The dotted lines give the approximations (6) and (13). For $N=1$ we present the diagonal case.

$$\left\langle \left(\frac{d\sigma_{ab}^{o}}{dE} \right)^2 \right\rangle = \frac{2\pi^2(\alpha'^2+\alpha'+2)}{(\alpha'-2)\alpha'^2(\alpha'+1)^2(\alpha'+3)} \times \left[(2-\beta)\frac{\alpha'+2}{\alpha'+1} + 4(\beta-1) \right]. \quad (12)$$

Here, $\alpha'=\beta(N+\Gamma/2)$.

For $\Gamma \gg 1$, based on the numerical simulations, we assume that $\widetilde{P}_\beta(d\sigma_{ab}/dE)$ is exponential and that for different pair of channels a and b the $d\sigma_{ab}/dE$ are uncorrelated. We then equate $\mu_\beta^2=2/\langle (d\sigma_{ab}^{d}/dE)^2\rangle$ and $\nu_\beta^2=2/\langle (d\sigma_{ab}^{o}/dE)^2\rangle$ to write

$$\widetilde{P}_\beta(dT/dE) = \frac{\mu_\beta^2\nu_\beta}{16}\left[\left(\frac{1}{\alpha_1}+\frac{1}{\alpha_2} \right)^2 \exp\left(-\frac{\nu_\beta}{2}\left|\frac{dT}{dE}\right| \right) + \left(\frac{1}{\alpha_1}-\frac{1}{\alpha_2} \right)\left(\frac{1}{\alpha_1}+\frac{1}{\alpha_2}+\frac{1}{\mu_\beta}+\left|\frac{dT}{dE}\right| \right) \times \exp\left(-\mu_\beta\left|\frac{dT}{dE}\right| \right) \right], \quad (13)$$

where $\alpha_1=\mu_\beta+\nu_\beta/2$, $\alpha_2=\mu_\beta-\nu_\beta/2$. Figure 6 compares the approximation $\widetilde{P}_\beta(dT/dE)$ with our numerical simulations. We chose parameters realistic to our experiment. The agreement is quite good. Deviations between the approximation (13) and the numerical simulations are of order $1/\Gamma$.

IV. STATISTICAL ANALYSIS OF THE EXPERIMENTAL RESULTS

The statistical analysis of our experiment is based on two central hypotheses. First, as standard, we assume that the transmission fluctuations of a chaotic system are the same as those predicted by random-matrix theory (RMT) [4]. Second, we employ an ergodic hypothesis to justify that ensemble averages are equivalent to running averages, that is, averages over the energy (frequency) and/or shape parameters. This requires RMT to be ergodic [42,43], which was recently shown [44]. A recent experimental microwave study [45] claims to circumvent the ergodic hypothesis by placing a perturbation (absorber) at different cavity positions, hence generating different realizations of the scattering system. However, the position of the perturbation can be regarded as a running variable. This means that Ref. [45] implicitly assumes that there are no spectral correlations as the absorber is moved. It was shown in Ref. [46] that such correlations exist as long as the range of the perturbation potential is small compared to the wavelength. In case this assumption is too strong, in practice, ergodicity justifies the statistical analysis either way.

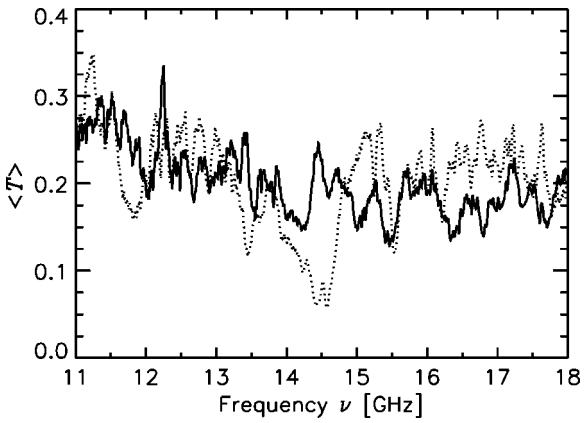

FIG. 7. Mean transmission $\langle T\rangle$ for the $N=2$ case for $B=0$ (solid line) and 0.470 T (dotted line). The Larmor resonance frequency is $\omega_R=2\pi\times 14.86$ GHz.

The experimental transmission coefficients were obtained by superimposing 100 different spectra measured for billiard lengths b (see Fig. 1). In the studied frequency regime there is only a single propagating mode in each of the waveguides. Hence, with every waveguide we associate a single scattering channel. For the $N=1$ case all measurements for the different combinations of entrance and exit waveguides were superimposed. The transmission for the $N=2$ case was obtained by combining the results from all $N=1$ measurements, namely, $T=T_{13}+T_{14}+T_{23}+T_{24}$.

Figure 7 shows the mean transmission ($N=2$ case) with and without applied external magnetic field. When related to experimental quantities, $\langle\cdots\rangle$ indicate running averages. The strong absorption due to the Larmor resonance is clearly seen. In the Appendix we discuss why the phase-breaking effect is expected to be best observed in the tails of the Larmor resonance. Figure 8 illustrates this very nicely. It shows the scaled transmission distribution $P(T/\langle T\rangle)$ for the asymmetric billiard in three different frequency windows both with and without applied external magnetic field. It is only in the frequency interval from 13.55 to 13.85 GHz that $P(T/\langle T\rangle)$ changes with magnetic field. We stress that this is different from just an absorption effect. In the frequency window around 14.45 GHz, where the absorption is strongest, the normalized distributions with and without magnetic field are basically the same (the only difference is in the mean transmission. We identify the change in $P(T/\langle T\rangle)$ with the expected phase-breaking effect and assume that the applied magnetic field is sufficient for the ferrite cylinders to

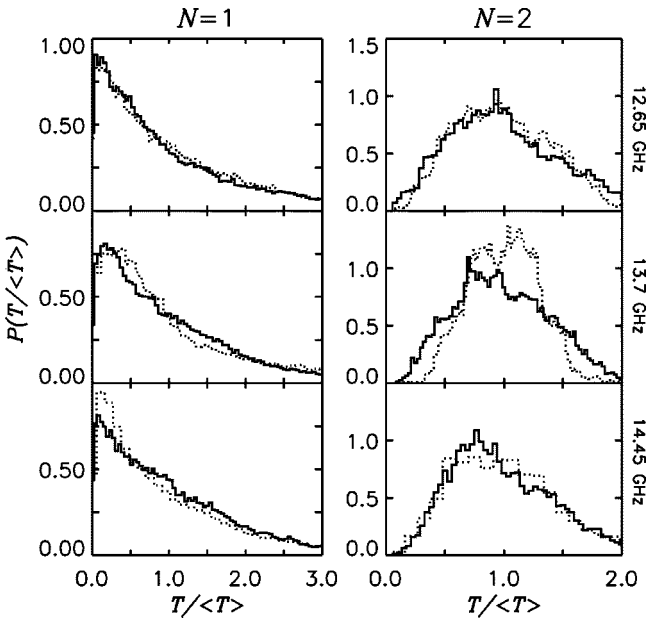

FIG. 8. Transmission distribution for the $N=1$ (left) and 2 (right) channel cases for three different frequency windows of width $\delta\nu=0.3$ GHz centered at ν_0 (indicated in the figure). The histograms correspond to $B=0$ (solid line) and 0.470 T (dotted line).

fully break time-reversal symmetry. Similar observations were made for the symmetric billiard.

Before we present our statistical analysis, it remains to discuss the coupling of the waveguides to the cavity. For that purpose we measured the transmission through two waveguides facing each other directly. In the whole applied frequency range the total transmission was unity, with an experimental uncertainty below 5%, showing that the antenna coupling is perfect. There are, however, reflections of about 10% in amplitude from the open ends of the waveguides, where they are attached to the billiard. Small deviations from ideal coupling are also consistent, for the frequencies we use, with Ref. [27]. Since the absorption is strong in the present experiment, and an imperfect coupling can be compensated for to a large extent by a rescaled absorption constant, we decided not to explicitly account for coupling corrections. In summary, throughout the forthcoming analysis we assume perfect coupling between the cavity and the waveguides.

For the sake of clarity, we present the statistical analysis of the asymmetric and the symmetric cavities separately.

Asymmetric cavity distributions

Figure 9 compares the experimental transmission distributions in the "phase-breaking" frequency window with the statistical theory. The absorption parameter Γ (see Sec. III) was adjusted to give the best fit of the theoretical $\langle T\rangle$ to the experiment. Note that in the frequency scale where the universal transmission fluctuations occur the mean transmission is a smooth function. It also does not show noticeable changes within the "phase-breaking" window (see Fig. 7). The agreement between experiment and theory for $P(T)$ is excellent, except for $N=2$ with $B\neq 0$ [47].

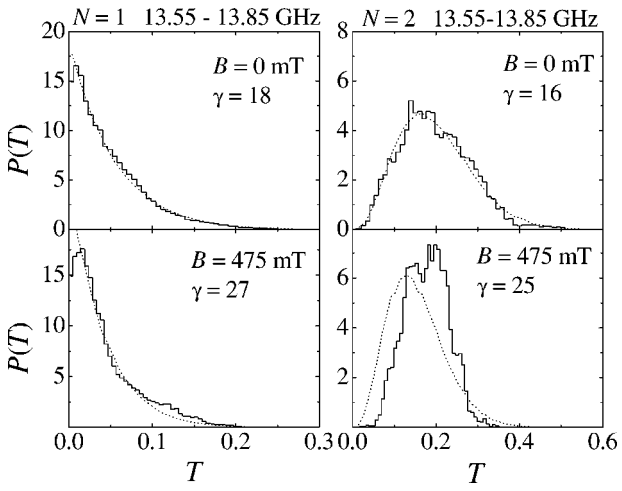

FIG. 9. Transmission distributions for the asymmetric cavity. The histograms correspond to data taken within the indicated frequency window. The dotted lines stand for the random-matrix simulations, with Γ as a fitting parameter.

We work with a single asymmetric cavity, but use different Γ values for $N=1$ and 2. The reason is simple: For $N=2$ we consider the contributions from all antennas to the transmission, whereas for $N=1$ two antennas act as additional absorption channels. This gives rise to a simple relation, namely, $\Gamma^{(N=1)}=\Gamma^{(N=2)}+2$.

To obtain the experimental distribution of the transmission energy derivative $\widetilde{P}(dT/dE)$ we introduce $E=\nu/\Delta$, which measures the frequency ν in units of the mean resonance spacing Δ given by the Weyl formula. Figure 10 shows a comparison between theoretical and experimental results for $\widetilde{P}(dT/dE)$. Note that we take the same Γ as for $P(T)$. The signatures of the channel number, and the influence of time-reversal symmetry breaking are clearly seen. We checked that the increase in absorption when switching on the magnetic field, without switching to the unitary ensemble as well, is not sufficient to reproduce the data. Inaccuracies in the assessment of the mean level resonance from

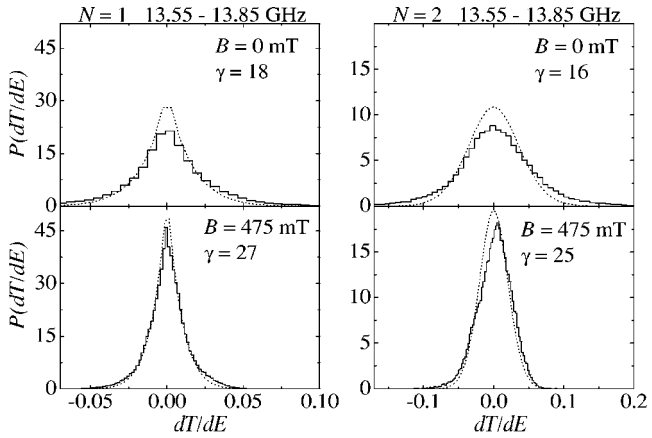

FIG. 10. Distribution of the energy derivative of the transmission for the asymmetric cavity, $\widetilde{P}(dT/dE)$. The dotted lines correspond to the theoretical distributions.

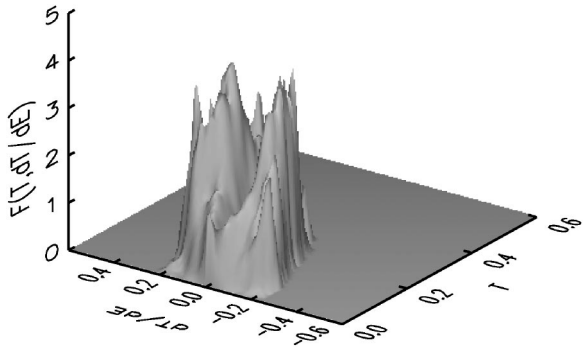

FIG. 11. Normalized joint distribution $F(T,dT/dE) = P(T,dT/dE)/[P(T)\widetilde{P}(dT/dE)]$ for the asymmetric cavity for $N=1$, $B=0$. A similar result holds for $B\neq 0$.

the Weyl formula provide a possible explanation for the slight disagreement between theory and experiment. The Weyl formula does not account for the standing waves in the ferrite cylinders and, thus, overestimates the mean resonance spacing. This is consistent with Fig. 10.

The joint distribution of T and dT/dE was studied in Ref. [18] for $N=1$ and $\Gamma=0$. Remarkably, it was found that albeit T and dT/dE are correlated, the rescaled quantity $(dT/dE)_{\mathrm{resc}}=(dT/dE)/\sqrt{T(1-T)}$ and T are not. We checked if this finding holds in our experiment, despite absorption. Figure 11 shows the "normalized" joint probability

$$F\left(T,\frac{dT}{dE}\right)\equiv\begin{cases}\dfrac{P(T,dT/dE)}{P(T)\widetilde{P}(dT/dE)} & \text{for } P(T)\widetilde{P}(dT/dE)\neq 0,\\ 0 & \text{for } P(T)\widetilde{P}(dT/dE)=0\end{cases} \tag{14}$$

in a three-dimensional representation for $N=1$ and $B=0$. Clear correlations are observed. In contrast, Fig. 12 shows $F[T,(dT/dE)_{\mathrm{resc}}]$. Here the distribution becomes flat, except for a couple of bins with few counts. Unfortunately we do not have enough statistics to make a more reliable determination of the joint distribution F. A similar result, not shown here, holds for the $B\neq 0$ case.

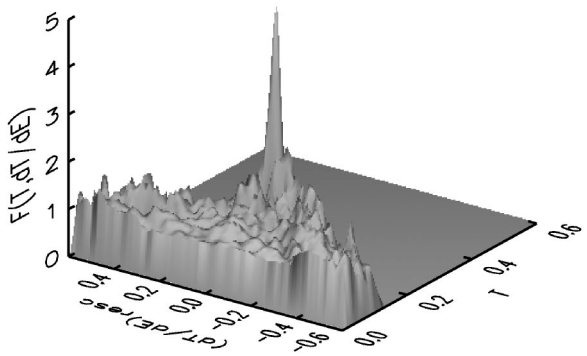

FIG. 12. Same as in Fig. 11, but with dT/dE replaced by $(dT/dE)_{\mathrm{resc}}=(dT/dE)/\sqrt{T(1-T)}$.

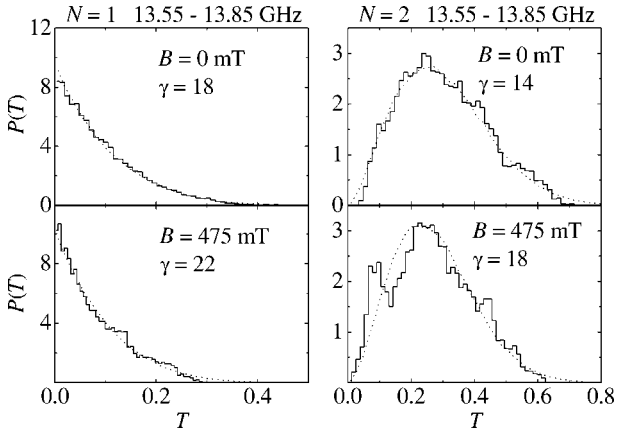

FIG. 13. Transmission distributions $P(T)$ for the symmetric billiard. Histograms stand for the data taken at the indicated frequency interval, whereas the dotted lines correspond to the simulations. The absorption Γ is a fitting parameter.

Symmetric cavity distributions

We switch now to the statistical analysis of the symmetric cavity transmission fluctuations.

Figure 13 shows the experimental shows $P(T)$ for transmissions within $13.55\leqslant\nu\leqslant 13.85$ GHz, where the phase-breaking effect is expected to be strongest. As before, the absorption parameter Γ is the best fit of the theory to the experiment. Here, for all studied cases a nearly perfect agreement is found. Now $\Gamma^{(N=1)}=\Gamma^{(N=2)}+4$. This is due the reflection symmetry.

Figure 14 shows the experimental distributions $P(dT/dE)$ for the symmetric case. The signatures of the channel number and the influence of breaking time-reversal symmetry are clearly seen. For all cases of the symmetric billiard the theoretical curves are plotted as well. We observe that the experimental distributions verify the overall trends of the theoretical predictions. In particular, the characteristic cusp at $E=0$ is nicely reproduced for $N=1$. Similar to the asymmetric case, the agreement between experiment and theory is not as good as for the transmission distribution.

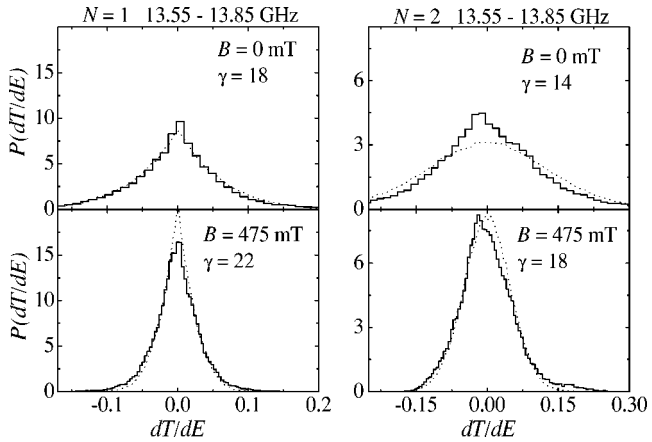

FIG. 14. Distribution of the energy derivative of the transmission for the symmetric cavity. The dotted lines corresponds to the theoretical distributions obtained from random-matrix theory.

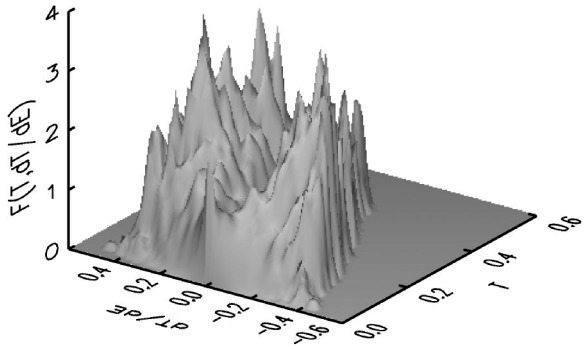

FIG. 15. Normalized joint distribution $F(T,dT/dE) = P(T,dT/dE)/[P(T)\widetilde{P}(dT/dE)]$ for the symmetric cavity for $N=1$, $B=0$. A similar result holds for $B\neq 0$.

In analogy to the case of asymmetric cavities, we investigate if the rescaled quantity $(dT/dE)_{\mathrm{resc}} = (dT/dE)/\sqrt{T(1-T)}$ is independent of T. Figure 15 shows the normalized joint probability $F(T,dT/dE)$, defined as in Eq. (14), in a three-dimensional representation for $N=1$ and $B=0$. A clear correlation is manifest. For comparison, Fig. 16 shows the corresponding histogram for $F(T,(dT/dE)_{\mathrm{resc}})$. The scaled F becomes flat, except for a few bins with low counting. This indicates that the rescaled joint probability distribution F is very well described as a product of $P(T)$ and $\widetilde{P}[(dT/dE)_{\mathrm{resc}}]$. We conclude that if there are correlations between T and $(dT/dE)_{\mathrm{resc}}$, they are very small. We observe similar results, not shown here, for the $B\neq 0$ case.

V. CONCLUSIONS

This work shows that microwaves are ideally suited to experimentally verify the theory of universal transmission fluctuations through chaotic cavities. The results presented in the present paper would have been hardly accessible by any other method.

We observe a nice overall agreement between our experimental data and the random-matrix results. However, the comparison between theory and microwave experiment is limited by the following issues.

In experiments, the coupling between waveguides and the cavity is usually not ideal, whereas in most theoretical works

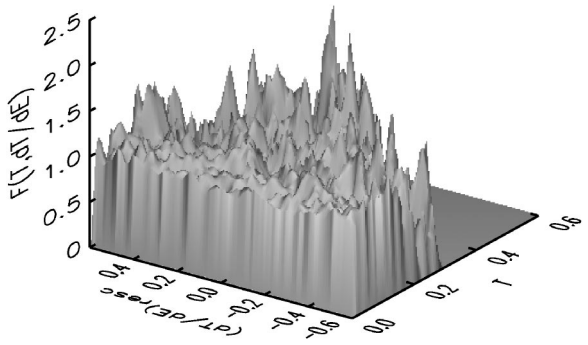

FIG. 16. Same as in Fig. 15, but with dT/dE replaced by $(dT/dE)_{\mathrm{resc}} = (dT/dE)/\sqrt{T(1-T)}$.

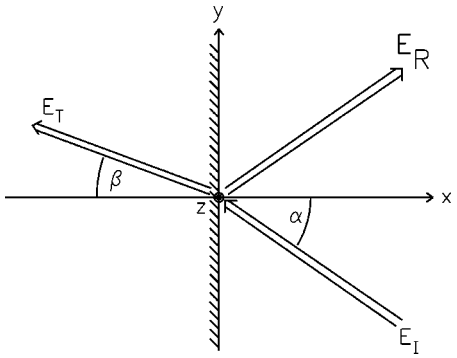

FIG. 17. Plane wave reflected by the surface of a ferrite slab.

ideal coupling is assumed. In the frequency range studied here, the working hypothesis of nearly perfect coupling is supported by Ref. [27]. In general, however, it turns out that without measuring the S matrix (with phases) it is hard to disentangle direct reflection at the cavity entrance (imperfect coupling) from absorption. From the experimental side, it would be desirable to have a better handle on absorption.

Microwave systems are usually time-reversal invariant, and as we have seen it is not trivial to break this symmetry. At the same time we increase the magnetic field, turning on the phase-breaking mechanism, absorption also increases. Unfortunately, both effects are inextricable. This is why it is beyond our present experimental capability to quantitatively investigate the transmission fluctuations along the crossover regime between preserved and broken time-reversal invariance. Actually, to compare theory with experimental results we assume that the transmission data at $B=0.470$ mT and $13.55<\nu<13.85$ GHz are far beyond the crossover regime.

We hope that the present work will trigger additional theoretical effort in the mentioned directions.

ACKNOWLEDGMENTS

C. W. J. Beenakker is thanked for numerous discussions at different stages of this work. We also thank P. A. Mello for suggesting the symmetric cavities measurements. The experiments were supported by the Deutsche Forschungsgemeinschaft. M.M.M. was supported by CLAF-CNPq (Brazil) and C.H.L. by CNPq (Brazil).

APPENDIX: PHASE-BREAKING PROPERTIES OF THE FERRITE

This Appendix is devoted to the discussion of the ferromagnetic resonance and the phase-breaking mechanism. For that purpose we first quickly present some elements of the well-established theory of microwave ferrites; see for instance, Ref. [39].

For the sake of simplicity, we first restrict ourselves to the situation of an incoming plane wave reflected by the surface of an semi-infinite ferrite medium. We assume that incoming, reflected, and refracted waves propagate in the xy plane and are polarized along the z direction, and that there is an externally applied static magnetic field in the z direction, as shown in Fig. 17. We ask for the phase acquired due to the

reflection on the ferrite.

To answer this question we need to solve Maxwell's equations. For this geometry and single-frequency electromagnetic fields, like our microwaves, this is a simple task. The ferrite properties come into play via the constitutive relations $\mathbf{D}=\epsilon_0\epsilon\mathbf{E}$ and $\mathbf{B}=\mu_0\mu\mathbf{H}$; more specifically through the permeability μ, which is a tensor with the form

$$\mu = 1 + \chi = \begin{pmatrix} 1+\chi_r & -i\chi_i & \cdot \\ i\chi_i & 1+\chi_r & \cdot \\ \cdot & \cdot & 1+\chi_0 \end{pmatrix} \tag{A1}$$

with

$$\chi_r = \frac{\omega_L\omega_M}{\omega_L^2 - \hat{\omega}^2}, \quad \chi_i = -\frac{\hat{\omega}\omega_M}{\omega_L^2 - \hat{\omega}^2}, \quad \hat{\omega} = \omega + i\lambda. \tag{A2}$$

Here $\omega_L=-\gamma H_0$ and $\omega_M=\gamma M_0$ are the precession angular frequencies about the external field H_0 and the equilibrium magnetization M_0, respectively. μ_0 is the static susceptibility. Here λ is the rate that characterizes the decay of the magnetization toward its thermal equilibrium due to spin-spin and spin-lattice interactions within the ferrite. More details can be found, for instance, in Chap. 2.2.3 of Ref. [40].

We solve the proposed problem using for the electric field the ansatz $\mathbf{E}(r)=E(r)\mathbf{e_z}$, where

$$E(r) = \begin{cases} E_T e^{i\mathbf{k}_T\cdot\mathbf{r}}, & x<0, \\ E_I e^{i\mathbf{k}_I\cdot\mathbf{r}} + E_R e^{i\mathbf{k}_R\cdot\mathbf{r}}, & x>0, \end{cases} \tag{A3}$$

with $\mathbf{k}_I=k_0(-\cos\alpha,\sin\alpha,0)$, $\mathbf{k}_R=k_0(\cos\alpha,\sin\alpha,0)$, $\mathbf{k}_T=k(-\cos\beta,\sin\beta,0)$ (see Fig. 17).

The derivation of the amplitudes E_I, E_R, and E_T is similar to that of Fresnel's formula (see, for instance, [41]). Since an explicit calculation for ferrites is performed in Ref. [31], only the results will be given. Using the continuity of $\mathbf{E}_\parallel$, $\mathbf{D}_\perp$, $\mathbf{B}_\perp$, and $\mathbf{H}_\parallel$ on the boundary, one writes

$$E_T = E_I + E_R \quad \text{and} \quad k\sin\beta = k_0\sin\alpha \tag{A4}$$

which is just Snell's law. For the relative amplitude of the reflected part we obtain

$$\frac{E_R}{E_I} = \frac{(n^2/\epsilon)\cos\alpha + i\delta\sin\alpha - \sqrt{n^2-\sin^2\alpha}}{(n^2/\epsilon)\cos\alpha - i\delta\sin\alpha + \sqrt{n^2-\sin^2\alpha}} \tag{A5}$$

where

$$n^2 = \frac{(\omega_L+\omega_M)^2 - \hat{\omega}^2}{\omega_L(\omega_L+\omega_M) - \hat{\omega}^2} \tag{A6}$$

and

$$\delta = \frac{\chi_i}{1+\chi_r} = -\frac{\hat{\omega}\omega_M}{\omega_L(\omega_L+\omega_M) - \hat{\omega}^2}. \tag{A7}$$

Note that there is a term depending on the sign of α, i.e., on the direction of the incident wave. This term is responsible for the phase-breaking effect.

The above formulas have to be modified when dealing with a ferrite of finite width. For a slab of thickness l and $\alpha=0$ we have

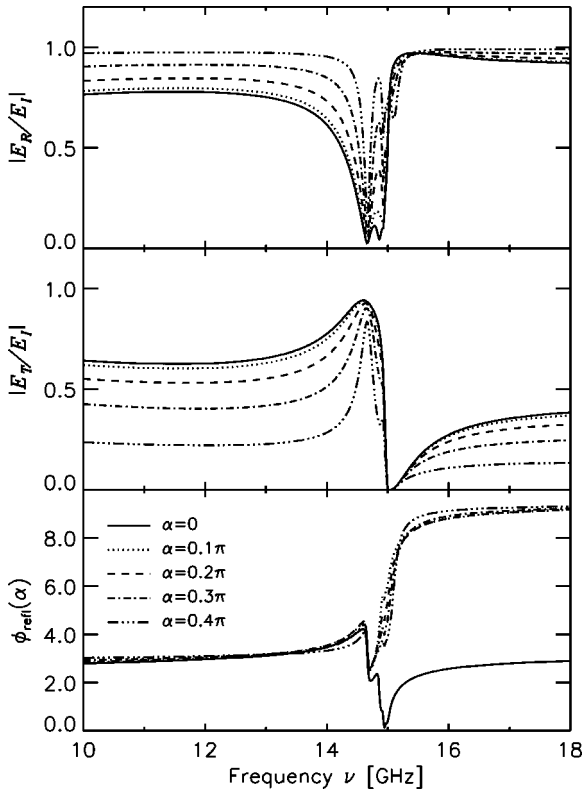

FIG. 18. Reflection, transmission, and phase shift for a ferrite slab ($M_0=130$ mT, $\epsilon=15$, $\lambda=0.1$ GHz) of thickness $l=1$ mm at $B_0=\mu_0H_0=470$ mT for different incidence angles α.

$$\frac{E_T}{E_I} = \frac{4\epsilon/n}{(1+\epsilon/n)^2 e^{ik(1-n)l} - (1-\epsilon/n)^2 e^{ik(1+n)l}} \tag{A8}$$

and

$$\frac{E_R}{E_I} = -2i\sin knl \frac{1-\epsilon^2/n^2}{(1+\epsilon/n)^2 e^{ik(1-n)l} - (1-\epsilon/n)^2 e^{ik(1+n)l}}. \tag{A9}$$

In contrast to Eq. (A5), E_T is no longer the amplitude of the transmitted wave propagating inside the ferrite. Here E_T is the amplitude of the wave that crossed the ferrite slab and emerged at the other side. The explicit formula for $\alpha\neq 0$ is lengthy and is not presented here.

The phase breaking becomes clearly manifest by writing Eq. (A9) as

$$\frac{E_R}{E_I} = \left|\frac{E_R}{E_I}\right| e^{i\phi_{\text{refl}}(\alpha)} \tag{A10}$$

where $\phi_{\text{refl}}(\alpha)$ is the phase acquired due to reflection. Figure 18 shows the modulus of transmission $|E_T/E_I|$ and reflection $|E_R/E_I|$ as well as the phase shift for different incidence angles and $l=1$ mm, the thickness of our ferrite cylinders. The curves are calculated using the ferrite parameters (see caption of Fig. 18) given by the supplier. We find a resonance angular frequency of $\omega_R=\sqrt{\omega_L(\omega_L+\omega_M)}=2\pi\times 14.86$ GHz. This resonance corresponds to the dominant structure ob-

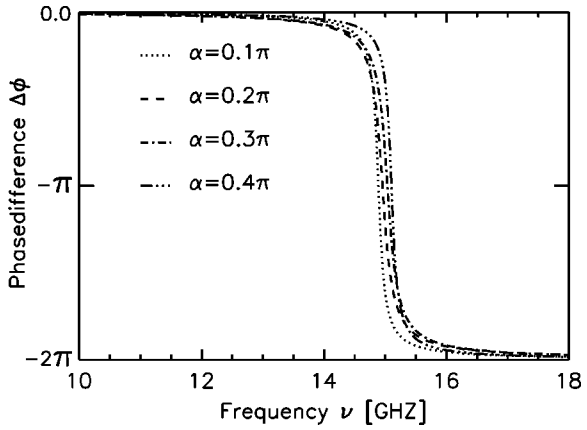

FIG. 19. Difference $\Delta\phi=\phi_{\mathrm{refl}}(\alpha)-\phi_{\mathrm{refl}}(-\alpha)$ of phase shifts observed between an incoming wave and its time-reversed equivalent.

served in Fig. 18. The additional substructures are due to standing waves inside the ferrite.

To illustrate the phase-breaking effect of the ferrite, in Fig. 19 we show the phase difference $\Delta\phi=\phi_{\mathrm{refl}}(\alpha)-\phi_{\mathrm{refl}}(-\alpha)$ between the incoming and the time-reversed wave. We see that the effect is maximal at the resonance frequency, and vanishes as one moves off resonance. Unfortunately, the absorption is maximal at the resonance too. These are the quantitative observations in support of the discussion presented in Sec. II.

Finally, to experimentally check the properties of the ferrites, we place a small sheet of the material between two waveguides facing each other. Two different thicknesses $l=1$ and 2 mm were used. Figure 20 shows the measured reflection $|E_R/E_I|$ as a function of ν. The small oscillations superimposing the dominant resonance structures correspond to standing waves within the waveguide and are an artifact of the experiment. Comparing the experimental results with the calculation shown in Fig. 18, we notice that the assumption of a single homogeneous internal magnetization is not in accordance with the measurement. The dashed line is obtained by superimposing the theoretical results for two different values of the magnetization. The overall behavior of the resonance structures becomes then in qualitative agreement with the data. The different magnetizations are due to the domain structure of the ferrite. There is a critical magnitude of external magnetic field below which the magnetization is incomplete and each Weiss domain has a different magnetization. It is desirable to eliminate this feature by operating at larger magnetic fields. This is unfortunately not possible since (i) a larger magnetic field implies a larger Larmor frequency; (b) our goal to keep the equivalence with quantum mechanics limits our study to frequencies where the resonator is quasi-two-dimensional. In this respect the applied field we use is about the highest possible.

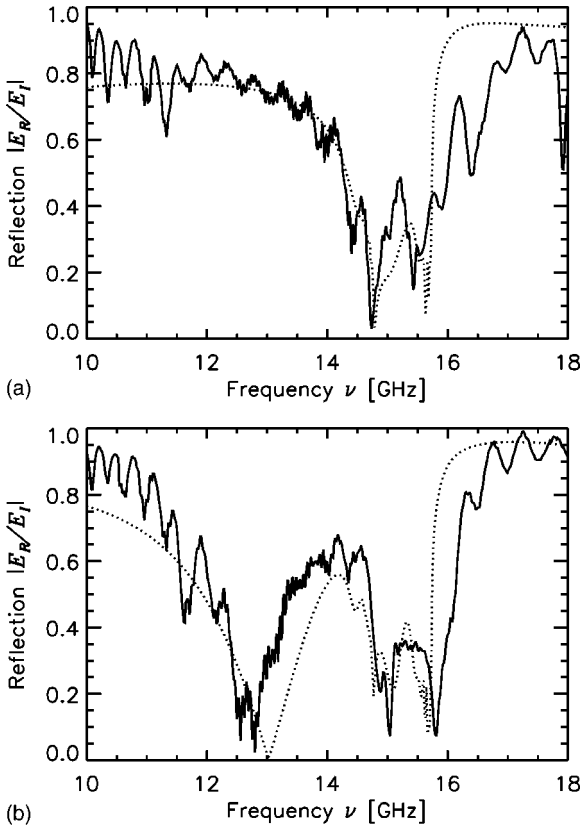

FIG. 20. Experimental reflection for a ferrite slab of thickness $l=1$ (a) and 2 mm (b). The dashed lines have been calculated by superimposing the results for two different internal magnetizations $M_0=110$ and 190 mT. The broad minimum observed for $l=2$ mm close to 13 GHz is due to a standing wave within the ferrite. For $l=1$ mm the corresponding minimum is at 15 GHz and overlapping with the ferromagnetic resonance.

[1] C. W. J. Beenakker, Rev. Mod. Phys. **69**, 731 (1997).
[2] T. Guhr, A. Müller-Groeling, and H. A. Weidenmüller, Phys. Rep. **299**, 189 (1998).
[3] R. Blümel and U. Smilansky, Phys. Rev. Lett. **64**, 241 (1990).
[4] C. H. Lewenkopf and H. A. Weidenmüller, Ann. Phys. (N.Y.) **212**, 53 (1991).
[5] E. Doron and U. Smilansky, Nucl. Phys. A **545**, 455c (1992).
[6] C. M. Marcus, A. J. Rimberg, R. M. Westervelt, P. F. Hopkins, and A. C. Gossard, Phys. Rev. Lett. **69**, 506 (1992).
[7] E. R. P. Alves and C. H. Lewenkopf, Phys. Rev. Lett. **88**, 256805 (2002); C. H. Lewenkopf, Chaos, Solitons Fractals **16**, 449 (2003).
[8] A. G. Huibers, M. Switkes, C. M. Marcus, K. Campman, and A. C. Gossard, Phys. Rev. Lett. **81**, 200 (1998).
[9] H. U. Baranger and P. A. Mello, Phys. Rev. B **51**, R4703 (1995).
[10] H. U. Baranger and P. A. Mello, Phys. Rev. Lett. **73**, 142 (1994).
[11] R. A. Jalabert, J.-L. Pichard, and C. W. J. Beenakker, Europhys. Lett. **27**, 255 (1994).

[12] A. G. Huibers, S. R. Patel, C. M. Marcus, P. W. Brouwer, C. I. Duruöz, and J. S. Harris, Jr., Phys. Rev. Lett. **81**, 1917 (1998).
[13] E. Doron, U. Smilansky, and A. Frenkel, Phys. Rev. Lett. **65**, 3072 (1990).
[14] R. A. Jalabert, H. U. Baranger, and A. D. Stone, Phys. Rev. Lett. **65**, 2442 (1990).
[15] H. Schanze, E. R. P. Alves, C. H. Lewenkopf, and H.-J. Stöckmann, Phys. Rev. E **64**, 065201(R) (2001).
[16] Y.-H. Kim, M. Barth, H.-J. Stöckmann, and J. P. Bird, Phys. Rev. B **65**, 165317 (2002); Y.-H. Kim, M. Barth, U. Kuhl, H.-J. Stöckmann, and J. P. Bird, *ibid.* **68**, 045315 (2003).
[17] S. A. van Langen, P. Silvestrov, and C. W. J. Beenakker, Stud. Appl. Math. **23**, 691 (1998).
[18] P. W. Brouwer, S. A. van Langen, K. M. Frahm, M. Büttiker, and C. W. J. Beenakker, Phys. Rev. Lett. **79**, 913 (1997).
[19] P. So, S. M. Anlage, E. Ott, and R. N. Oerter, Phys. Rev. Lett. **74**, 2662 (1995).
[20] U. Stoffregen, J. Stein, H.-J. Stöckmann, M. Kuś, and F. Haake, Phys. Rev. Lett. **74**, 2666 (1995).
[21] E. Kogan, P. A. Mello, and HeLiqun, Phys. Rev. E **61**, R17 (2000).
[22] C. W. J. Beenakker and P. W. Brouwer, Physica E (Amsterdam) **9**, 463 (2001).
[23] D. V. Savin and H.-J. Sommers, Phys. Rev. E **68**, 036211 (2003).
[24] D. V. Savin and H.-J. Sommers, Phys. Rev. E **69**, 035201(R) (2004).
[25] P. W. Brouwer, Phys. Rev. B **51**, 16878 (1995).
[26] D. V. Savin, Y. V. Fyodorov, and H.-J. Sommers, Phys. Rev. E **63**, 035202(R) (2001).
[27] R. A. Méndez-Sánchez, U. Kuhl, M. Barth, C. H. Lewenkopf, and H. J. Stöckmann, Phys. Rev. Lett. **91**, 174102 (2003).
[28] M. Martínez and P. A. Mello, Phys. Rev. E **63**, 016205 (2000).
[29] H. U. Baranger and P. A. Mello, Phys. Rev. B **54**, R14297 (1996).
[30] Reflection symmetry is limited by the workshop precision. We estimate it to be better than 0.1 mm, which is much smaller than the typical wavelengths of the experiment (centimeters). Uncertainties in the ferrite positions should be of the same order. We also neglect inhomogeneities in the ferrite.
[31] M. Vraničar, M. Barth, G. Veble, M. Robnik, and H.-J. Stöckmann, J. Phys. A **35**, 4929 (2002).
[32] P. A. Mello and H. U. Baranger, Waves Random Media **9**, 105 (1999).
[33] C. H. Lewenkopf, A. Müller, and E. Doron, Phys. Rev. A **45**, 2635 (1992).
[34] P. W. Brouwer and C. W. J. Beenakker, Phys. Rev. B **55**, 4695 (1997).
[35] J. J. M. Verbaarschot, H. A. Weidenmüller, and M. R. Zirnbauer, Phys. Rep. **129**, 367 (1985).
[36] P. W. Brouwer, K. M. Frahm, and C. W. J. Beenakker, Phys. Rev. Lett. **78**, 4737 (1997).
[37] M. Martínez-Mares, e-print cond-mat/0410746.
[38] V. A. Gopar, M. Martínez, P. A. Mello, and H. U. Baranger, J. Phys. A **29**, 881 (1996).
[39] B. Lax and K. Button, *Microwave Ferrites and Ferrimagnetics* (McGraw-Hill, New York, 1962).
[40] H.-J. Stöckmann, *Quantum Chaos—An Introduction* (Cambridge University Press, Cambridge, U.K., 1999).
[41] J. D. Jackson, *Classical Electrodynamics* (Wiley, New York, 1962).
[42] J. B. French, P. A. Mello, and A. Pandey, Phys. Lett. **80B**, 17 (1978).
[43] A. Pandey, Ann. Phys. (N.Y.) **119**, 170 (1979).
[44] Z. Pluhař and H. A. Weidenmüller, Phys. Rev. Lett. **84**, 2833 (2000).
[45] S. Hemmady, X. Zheng, E. Ott, T. M. Antonsen, and S. M. Anlage, e-print cond-mat/0403225.
[46] M. Barth, U. Kuhl, and H.-J. Stöckmann, Phys. Rev. Lett. **82**, 2026 (1999).
[47] In our previous publication [15] the agreement between theory and experiment for the $B=0.475$ T and $N=2$ case was better. This is due to a calibration problem, corrected in our current data analysis.